2004

Effect of Coil Geometry on Frost-Free Finned-Tube Evaporator Performance

Christian J. L. Hermes
Multibras Appliances

Marco E. Marques
Multibras Appliances

Claudio Melo
Federal University of Santa Catarina

Joaquim M. Goncalves
Federal Centre of Technological Education of Santa Catarina

EFFECT OF COIL GEOMETRY ON FROST-FREE FINNED-TUBE EVAPORATOR PERFORMANCE

C. J. L. HERMES[1], M. E. MARQUES[1], C. MELO[2], J. M. GONÇALVES[3]

[1] Multibrás Appliances S.A., Whirlpool Corporation
Rua Dona Francisca 7200, 89219-901, Joinville, SC, Brazil
+55 47 441 49 81, chermes@multibras.com.br

[2] Federal University of Santa Catarina, Department of Mechanical Engineering
P.O. Box 476, Florianópolis, SC, Brazil
+55 48 234 56 91, melo@nrva.ufsc.br

[3] Federal Centre of Technological Education of Santa Catarina
Rua Lino Kretzer 608, 88103-310, São José, SC, Brazil
+55 48 247 36 46, joaquim@sj.cefetsc.edu.br

ABSTRACT

This paper outlines a mathematical modelling approach to predict the steady-state behaviour of finned-coil evaporators. The model was built taking three domains into account: (i) refrigerant flow inside the coil; (ii) heat transfer through the walls; and (iii) air flow through the finned-coil array. The equations were obtained from the mass, momentum and energy conservation principles, mathematically written according to their one-dimensional differential formulation. Comparisons with experimental data were carried out and it was found that the model predictions, in terms of cooling capacity, refrigerant superheating, and outlet air temperature, were within an acceptable error band. The main contribution of this work is the thermal performance evaluation of two different evaporator designs under various operating conditions.

1. INTRODUCTION

Finned-coil evaporators are widely applied in household refrigerators in which automatic defrosting is a must. The example, shown in figure 1a, known as the 'continuous flat finned-coil evaporator', is commonly used in most of the frost-free appliances manufactured (Lee at al. 2002). In this type of evaporator the refrigerant circuit is arranged according to a 10-row, 2-column staggered array. In the first column, the refrigerant flow is top-down oriented while the air flows in the opposite direction. In the second column, both air and refrigerant flows are in the bottom-up direction.

If the evaporator is fulfilled with saturated refrigerant, i.e. there is no superheating at the coil outlet, a minor effect of the refrigerant circuit on the evaporator performance can be expected. However, this is not the case when significant superheating takes place within the coil. To get the most, in terms of heat transfer, from the coil geometry at any operation regime, a new evaporator design was patented (Hermes & Marques, 2002). The refrigerant now enters the heat exchanger through the A-port, and exits at the B-port, forming a pure counter-flow heat exchanger (see figure 1b). It should be noted that a pure parallel-flow evaporator may also be obtained by inverting the inlet and outlet ports.

This paper presents, discusses and validates a theoretical methodology to investigate the effect of refrigerant circuit on the thermal performance of frost-free finned-coil evaporators under different operating conditions: evaporating temperature, refrigerant mass flux, air flow rate, and inlet air temperature. Such parameters were combined according to a 2-level factorial design procedure (Box et al. 1978), forming a set of 2^4=16 numerical experiments for each coil geometry.

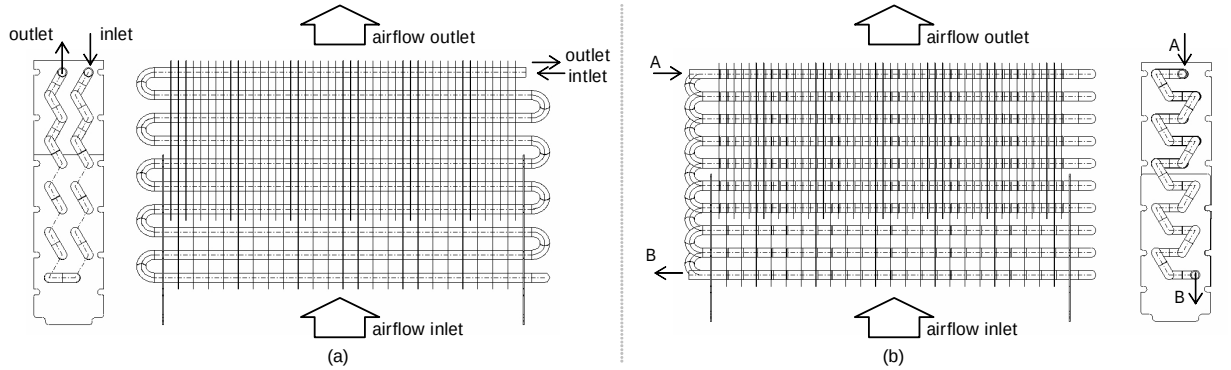

Figure 1: Finned-tube evaporators: (a) standard design; (b) proposed design

2. MATHEMATICAL MODEL

2.1 Simplifying Assumptions

The mathematical model was divided into three domains: (i) refrigerant flow inside the coil, (ii) heat transmission through the evaporator walls, and (iii) air flow through the finned-coil array. The air and refrigerant flows were modelled following a distributed approach, based on mass, momentum and energy balances applied to non-matching small control volumes centred at every connection between fin and coil. The modelling strategy was based on the following key assumptions:

- refrigerant flow steady, one-dimensional, viscous, and compressible
- viscous dissipation and heat diffusion effects neglected
- flow acceleration and kinetic energy variations neglected
- constant cross-sectional area and non-uniform fin distribution along the coil
- axial and radial heat diffusion along the coil wall neglected
- pure HFC-134a flow
- dry air

The premise behind the dry air assumption relies on the fact that most of the dehumidification process takes place during the start-up transient period. After that the air inside the refrigerated compartments becomes so dry that there is almost no latent heat to be transferred. Of course, this assumption is only valid if the rate of air infiltration through the door sealing is kept to a minimum.

2.2 Heat Transfer and Fluid Flow Equations

The refrigerant flow model was obtained from the momentum and energy conservation principles,

$$Adp + \tau_i dA_i = 0 \tag{1}$$

$$GAdh + q_i dA_i = 0 \tag{2}$$

The model for the dry air flow through the finned surfaces was obtained from the energy conservation law,

$$C_a V_a dt_a + q_o dA_o = 0 \tag{3}$$

The evaporator wall model was obtained from the following energy balance:

$$t_w = \left(\eta_i t_r dA_i + \eta_o t_a dA_o\right) / \left(\eta_i dA_i + \eta_o dA_o\right) \tag{4}$$

In these equations, h [J/kg], p [Pa], v [m^3/kg], $G=u/v$ [kg/s.m^2] and u [m/s] are the refrigerant enthalpy, pressure, specific volume, mass flux and flow velocity, respectively; $\tau_i=fGu/8$ is the shear stress at the internal walls [Pa]; $q_i=\eta_i(t_e-t_w)$ the heat flux absorbed by the refrigerant [W/m^2]; $q_o=\eta_o(t_a-t_w)$ the heat flux released by the air flow; t_e, t_w and t_a are the refrigerant, wall and air temperatures [K], respectively; η_i and η_o are the internal and external heat transfer coefficients [W/m^2.K], respectively; f is the friction-factor; C_a the air thermal capacity per unit of volume [J/m^{3}K]; and V_a is the air flow rate [m^3/s] through a differential portion of the coil. $dA_i=\pi D_i dl$ represents the differential refrigerant side surface area [m^2]; $A=\pi D_i^2/4$ the refrigerant side cross-sectional area [m^2]; and

$dA_o = \pi D_o dl + \eta_f dA_f$ the differential air side heat transfer area, where dA_f is the differential fin surface area and η_f the fin efficiency.

2.3 Thermodynamic and Thermophysical Properties

To complete the required set of equations, thermodynamic relations for the refrigerant temperature and specific volume as functions of pressure and enthalpy were needed. These were obtained from the REFPROP software (McLinden et al. 1998), and implemented according to a look-up table procedure in order to speed up the computation process. The dry air properties were calculated using polynomial fits proposed by ASHRAE (1976). The refrigerant two-phase flow properties were calculated considering the flow as homogeneous.

2.4 Empirical Relations

The refrigerant single-phase flow heat transfer coefficient was calculated using the so-called Dittus-Bölter equation, introduced by McAdams (1958). For evaporating flows the heat transfer coefficient correlation proposed by Wongwises et al. (2000) was adopted:

$$\eta_i / \eta_{lo} = 3.3775\, Xtt^{-0.6285} \tag{5}$$

where η_{lo} is the liquid-only heat transfer coefficient calculated by the Dittus-Böelter equation, and Xtt is the Lockhart-Martinelli parameter. Friction factors for both single- and two-phase flows were computed by Churchill's (1977) equation, using the liquid-only viscosity as the two-phase flow viscosity.

The air side heat transfer coefficient was calculated from the equation proposed by Karatas et al. (1998):

$$j = 0.138\, Re^{-0.281}\, \varepsilon^{-0.407} \tag{6}$$

where Re is the Reynolds number based on the coil outer diameter, j is the Colburn number, and ε is the relation between the overall air side heat transfer surface area ($=A_{to}+A_f$) and the tube-only surface area (A_{to}). The fin efficiency was computed according to Schmidt's procedure, as described by McQuinston & Parker (1994).

3. NUMERICAL SCHEME

The numerical procedure consists of approximating the ordinary differential equations by a forward differencing scheme. As all the differential equations are of first order, they may be solved by a one-way marching procedure starting with the inlet conditions. At the refrigerant side, the inlet conditions are the vapour quality, the mass flow rate, and the evaporating pressure. At the air side, the boundary conditions are the air flow rate and inlet temperature. Due to its implicitness, the resulting set of algebraic equations must be iteratively solved by successive substitutions. The convergence criteria were based on the relative and absolute errors between two successive iterations, requiring both to be smaller than 10^{-4}. Under-relaxation was also applied to improve the convergence robustness.

The computational grid was obtained by dividing the physical domain into 47 (x-axis), 10 (y-axis) and 2 (z-axis) control volumes, that yielded a total of 940 control volumes. It should be noted that the refrigerant flow is one-dimensional along the tube axis, l, whose origin is at the tube entrance. The indexes shown at the upper parts of the control volumes refer to the first column (z=1), while those located at the lower parts refer to the second column (z=2), as shown by figure 2. The air flow model is 1-D along the y-axis, although computations are also performed in the x and z directions.

To avoid a 3-D code implementation, the matrix indexes (i,j) were converted into a vector $l_1(i,j)$, using the refrigerant flow coordinates. Hence, for the first column (z=1), where the air and refrigerant flows are in opposite directions, the following conversion law was obeyed:

$$l_1(i,j) = \begin{cases} (m-j)n + i & \forall\, j \text{ even} \\ (m-j+1)n - i + 1 & \forall\, j \text{ odd} \end{cases} \tag{7}$$

For the second column (z=2), where the air and refrigerant flows are in the same direction, the conversion law assumed the following form:

$$l_2(i,j) = 2n.m + 1 - l_1(i,j) \tag{8}$$

The above conversion laws are only valid for the standard evaporator. A similar approach was also used for the proposed design. The flow properties were evaluated at the control surfaces, since the air and refrigerant grids are staggered. In addition, the control volume inlet conditions were taken as the *z*-axis average values of the air flow properties at the exit of the upstream control volumes. This gave a reasonable approximation since the air flow is under an intensive mixing process.

The solution algorithm is described below:

1. code initialisation: look-up table, mesh generation, inlet conditions computations
2. refrigerant flow computation (eq. 1,2), marching along the *l*-axis
3. tube wall temperature calculation (eq. 4)
4. air flow computations (eq. 3), marching along the *y*-axis
5. update of heat transfer coefficients and flow properties
6. return to step 2 until convergence is achieved

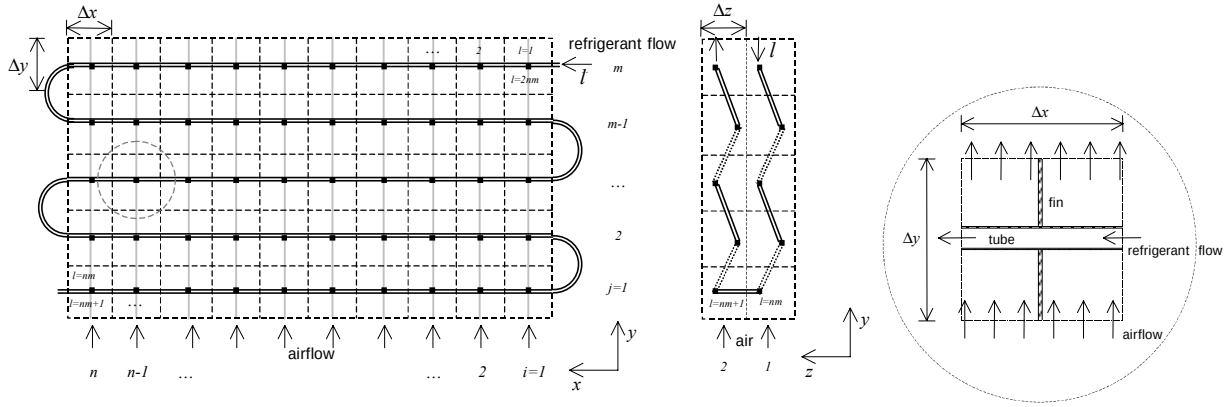

Figure 2: Computational grid for the standard design

4. MODEL VALIDATION

The model was validated against experimental data for the standard evaporator, obtained by Melo et al. (2004). The model input data are given by parameters #1 to #5, in table 1. Comparisons between measured and predicted cooling capacity, refrigerant superheating, and outlet air temperature are shown in table 2. It may be observed that the computational model predicts the cooling capacity and the outlet air temperature within error bands of ±5% and ±1°C, respectively. The refrigerant superheating is also predicted with a reasonable level of agreement of ±2°C. However, it is important to keep in mind that very few experimental data were available, and therefore a more comprehensive validation study is still needed.

Table 1: Experimental data from Melo et al. (2004)

#	Parameter	Unit	Test #1	Test #2	Test #3
1	Refrigerant inlet pressure	kPa	77.9	79.5	78.5
2	Refrigerant mass flow rate	kg/h	3.2	2.6	2.8
3	Inlet vapour-quality	%	42.7	43.2	43.0
4	Air flow rate	m^3/h	50.5	50.8	49.3
5	Inlet air temperature	°C	-20.7	-11.4	-14.8

Table 2: Comparisons with experimental data from Melo et al. (2004)

		Test#1			Test#2			Test#3		
Parameter	**Unit**	**Exp.**	**Calc.**	**Diff.**	**Exp.**	**Calc.**	**Diff.**	**Exp.**	**Calc.**	**Diff.**
Cooling capacity	W	122.0	116.2	-3.9%	102.4	100.2	-2.0%	111.1	107.6	-2.8%
Superheating degree	°C	8.1	6.3	-1.8	18.8	20.4	1.7	15.5	16.2	0.8
Outlet air temperature	°C	-26.7	-26.4	0.3	-16.5	-16.3	0.1	-20.5	-20.2	0.2

5. NUMERICAL EXPERIMENTS

The numerical experiments were planned according to a 2-level factorial design (Box et al. 1978). The inlet evaporating temperature ($t_{e,i}$), refrigerant mass flow rate (w), air inlet temperature ($t_{a,i}$), and the air flow rate (V_a) were chosen as the independent parameters. The inlet vapour quality was maintained at 25%. The upper and lower levels for each of the independent parameters are given in table 3. A total of 2^4=16 computer runs were performed for each of the three coil designs: (a) standard, (b) counter-flow, and (c) parallel-flow.

Table 3: Factorial design levels

#	Parameter	Unit	Lower level (-)	Upper level (+)
1	Inlet evaporating temperature, $t_{e,i}$	°C	-35	-25
2	Refrigerant mass flow rate, w	kg/h	2.0	4.0
3	Air inlet temperature, $t_{a,i}$	°C	-15	-9
4	Air flow rate, V_a	m^3/h	30	50

The cooling capacity, outlet air temperature, and refrigerant superheating were taken as the dependent variables. In order to establish a comparative criterion to analyse evaporator performance, the dependent parameters were combined into an overall heat transfer coefficient, UA, defined as follows:

$$UA = C_a V_a \left(\frac{t_{a,i} - t_{a,o}}{t_{a,i} - t_{e,min}} \right) \tag{9}$$

where $t_{e,min}=t_{e,o}-\Delta t_{sup}$. As expected the overall thermal conductance of the heat exchanger (UA) is improved when the cooling capacity tends to a maximum and the superheating (Δt_{sup}) to a minimum. It may also be noted that the refrigerant pressure drop decreases the UA value, since it decreases the minimum refrigerant temperature.

Figure 3 shows the relationship between the dependent and independent variables for each heat exchanger configuration. Only the main effects and first order interactions are plotted, since higher order interactions have shown a minor influence. These effects are the deviations of the positive setting for the respective factor from the overall mean. The most important factors affecting evaporator performance are the refrigerant mass flow rate and the evaporating temperature, as both have an important role on reducing the refrigerant superheating (see figure 3b). The effect of mass flow rate is quite obvious but special attention has to be given to the evaporating temperature, since an augmentation of this parameter leads to lower superheating and higher thermal conductance values.

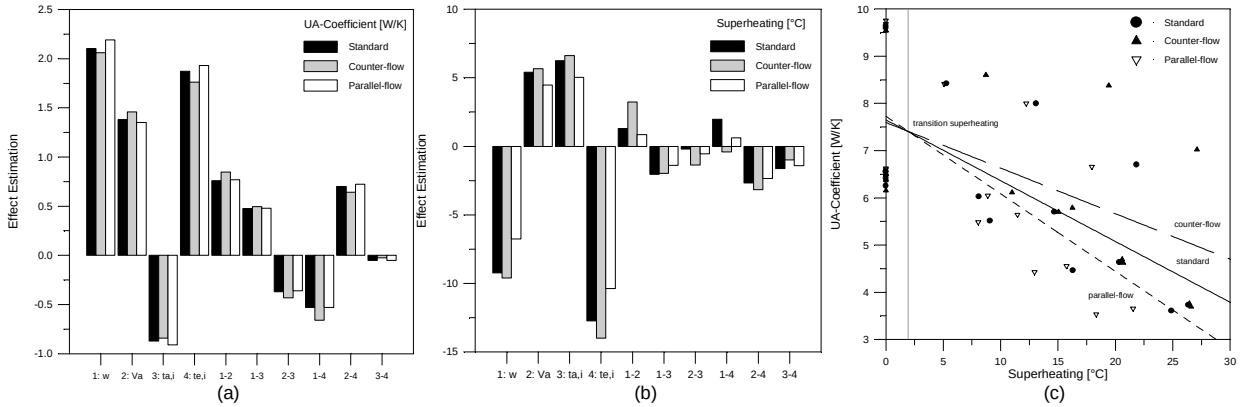

Figure 3: Factorial analysis results: (a) UA-coefficient; (b) superheating; (c) UA vs superheating

Figure 3c shows a plot of UA versus superheating considering all the data generated during the numerical experiments. As can be seen the fitting lines cross each other at a superheating value close to 2°C. This means that the parallel-flow configuration will perform better at lower superheating values and the counter-flow configuration at higher superheating values. Such behaviour can be better explained by figures 4 and 5, where the air and refrigerant temperature profiles along the coil length are shown for the (a) standard, (b) counter-flow, and (c) parallel-flow configurations. Figures 5 and 6 were plotted with the same input data ($t_{e,i}$=–31°C, x_i=34%, $t_{a,i}$=–15°C, V_a=50m^3/h), but with two different refrigerant mass flow rates, 5.2 and 3.2 kg/h, respectively.

With a mass flow rate of 5.2 kg/h, the evaporator is completely filled with saturated refrigerant, and therefore no superheating takes place within the coil. Figure 4a shows that in the first half of the standard evaporator the flow follows a counter-flow arrangement but the temperature profiles reflect a parallel-flow behaviour. In the second part of the evaporator a similar, but contrary behaviour is observed. This fact can be explained by the pressure drop at the refrigerant side that decreases the evaporating temperature. Following this reasoning, it is quite simple to understand the behaviour of the counter-flow (figure 4b) and parallel-flow (figure 4c) arrangements.

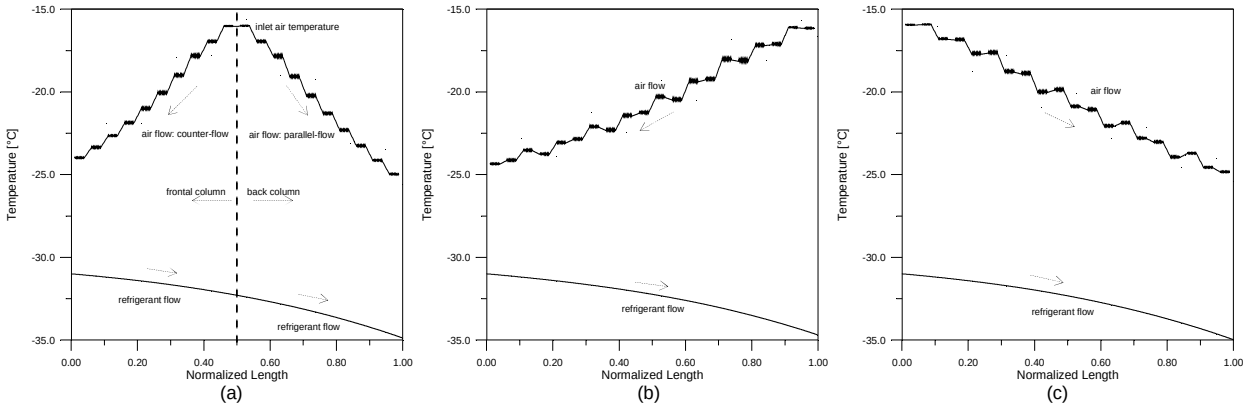

Figure 4: Temperature profiles with saturated refrigerant at the evaporator exit:
(a) standard; (b) counter-flow; (c) parallel-flow

With a mass flow rate of 3.2 kg/h, the refrigerant is completely evaporated inside the heat exchanger, and therefore some vapour superheating takes place at the evaporator exit. In this situation each heat exchanger configuration presents at least two distinct regions in terms of temperature profiles. In the standard arrangement three different regions can be observed (see figure 5a): (i) a parallel-flow temperature profile in the first half of the coil; (ii) a counter-flow temperature profile between the middle of the coil and the point of complete dry-out; and (iii) a parallel-flow temperature profile between the point of complete dry-out and the evaporator exit. In the counter-flow evaporator (figure 5b) two different regions may be observed: a parallel-flow temperature profile before the refrigerant dry-out and a counter-flow temperature profile after the refrigerant dry-out. A similar but contrary behaviour is shown in figure 5c for the parallel-flow design.

Hence, for low superheating values the parallel-flow evaporator behaves just like a pure counter-flow heat exchanger, and therefore presents the best *UA* value. The counter-flow evaporator, on the other hand, behaves just like a pure parallel-flow heat exchanger, and therefore presents a lower *UA* value. The standard evaporator presents an intermediate behaviour, as its circuit is part-parallel and part-counter-flow. As expected, the counter-flow evaporator performance improves with the superheating degree.

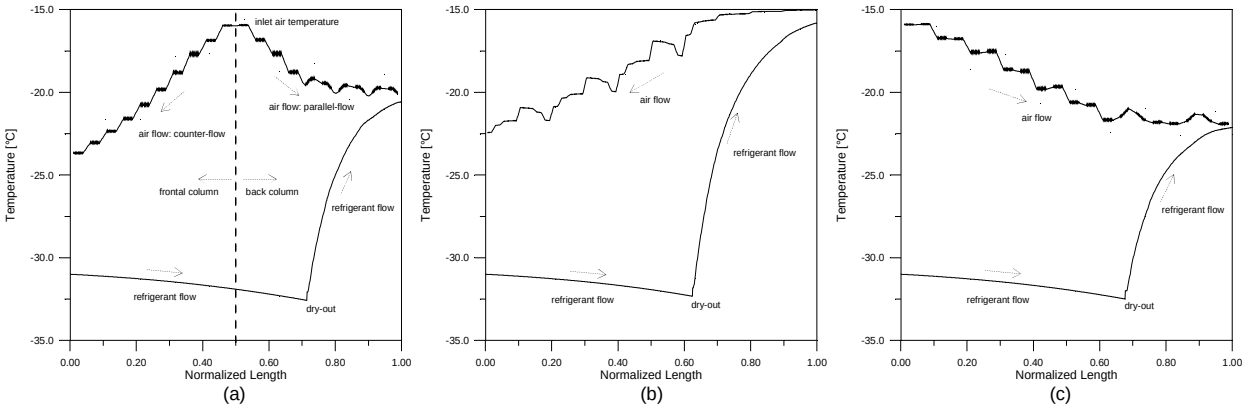

Figure 5: Temperature profiles with superheated refrigerant at the evaporator exit:
(a) standard; (b) counter-flow; (c) parallel-flow

In order to better illustrate the combined effect of refrigerant superheating and pressure drop on the evaporator performance, two additional cases were analysed, with (#1) and without (#2) pressure drop at the refrigerant side. The analysis was carried out by varying the refrigerant mass flow rate from zero up to 6 kg/h and maintaining the other input data constant at: $t_{e,i}$=–31°C, x_i=34%, V_a=50 m^3/h, $t_{a,i}$=–15°C. The results are illustrated in figure 6, where the 'black' and 'red' colours refer to cases #1 and #2, respectively.

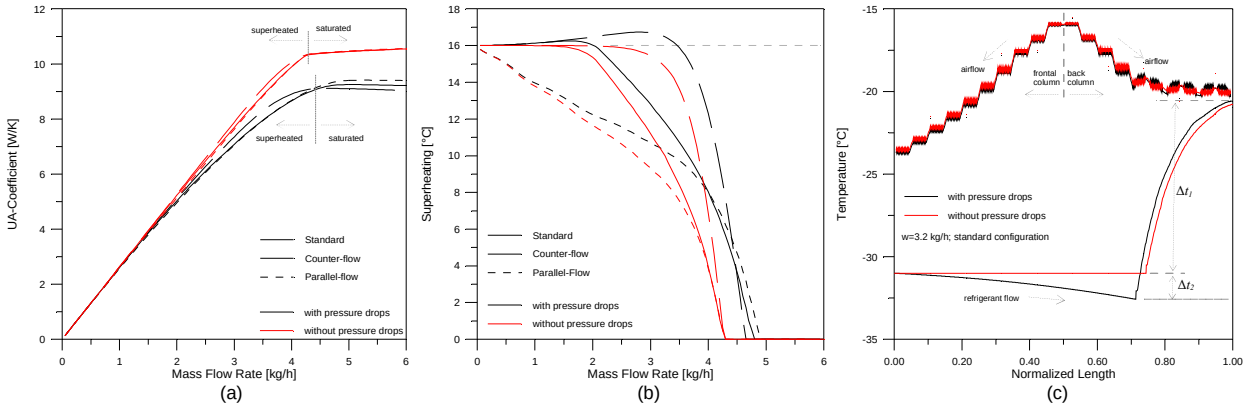

Figure 6: Effect of pressure drop: (a) *UA*-coefficient; (b) superheating; (c) temperature profiles

Figure 6a shows that in spite of the pressure drop the counter-flow evaporator offers the best thermal conductance when superheating occurs (mass flow rate below 4.3 kg/h). Under this condition the thermal performances of the parallel-flow and the standard evaporators are quite similar. At a mass flow rate of 3.5 kg/h, the *UA* value of the counter-flow evaporator is 5% higher than that of the standard evaporator. Once the coil is filled with saturated refrigerant, different behaviours may be observed, depending on the pressure drop. Without the pressure drop, there is no performance difference between the evaporators. With the pressure drop, the parallel-flow evaporator shows a higher *UA* value, followed by the standard and then by the counter-flow evaporator. The most significant difference appears at 6 kg/h, when the *UA* value of the parallel-flow evaporator becomes 2% and 4% higher than those of the standard and counter-flow designs, respectively. As expected, this difference tends to increase with the pressure drop.

Figure 6b shows the refrigerant superheating as a function of the mass flow rate. With and without the pressure drop, the superheating tends to 16°C, for all the evaporator arrangements, when the mass flow rate tends to zero. The superheating variation with mass flow rate, however, changes with the evaporator type and with the pressure drop. Figure 6c shows the pressure drop effect on superheating. Without the pressure drop the superheating is given by Δt_1, and with the pressure drop by $\Delta t_1+\Delta t_2$, where $\Delta t_2=t_{sat}(p_{inlet})-t_{sat}(p_{dry\text{-}out})$ is exclusively due to the pressure drop.

Figure 6c also shows that the dry-out position is affected by the refrigerant pressure drop. With the pressure drop the dry-out occurs along close to 71.5% of the coil length, and without the pressure drop close to 74.5%. This means an absolute difference of 210 mm for a 7.0 m length coil. This happens partly because the pressure drop increases the temperature difference between the air and the refrigerant sides, and partly because the pressure drop decreases the latent heat of vaporisation. Thus the combined effect is a reduction in the saturated coil length with the refrigerant pressure drop.

6. CONCLUDING REMARKS

A computer model to predict the air and refrigerant side temperature distributions along finned-coil evaporators was developed and validated against experimental data. The model predictions in terms of cooling capacity and outlet air temperature were within error bands of ±5% and ±1°C, respectively. Each simulation required a CPU time of 2s, using a Pentium Xeon 2.8GHz 1.5Mb RAM.

The model was also used to assess the performance capabilities of two evaporator designs, the standard and that proposed by Hermes & Marques (2002). The main conclusions are as follows:

- The refrigerant pressure drop along the coil length plays a crucial role in the evaporator performance. In the absence of superheating the counter-flow heat exchanger behaves like a parallel-flow one, and vice-versa. In these situations, the parallel-flow evaporator offers the best performance, followed by the standard and then by the counter-flow arrangement;
- With superheating, part of the evaporator is subject to a counter-flow and part to a parallel-flow temperature profile, regardless of the coil arrangement. In fact, three distinct regions were observed in the standard evaporator: (i) a parallel-flow temperature profile in the first half of the coil, (ii) a counter-flow temperature profile between the middle of the coil and the point of complete dry-out; and (iii) a parallel-flow temperature profile between the point of complete dry-out and the evaporator exit. Two regions were observed in the counter-flow design: a parallel-flow temperature profile before the refrigerant dry-out and a counter-flow temperature profile after the refrigerant dry-out. A similar but contrary behaviour was observed for the parallel-flow arrangement;
- A transition superheating value was found for some operating conditions and mass flow rates. At lower superheating values, the parallel-flow heat exchanger offered the best performance. At higher superheating values, the best performance was offered by the counter-flow design;
- For further conclusions, a transient analysis is strongly recommended.

REFERENCES

ASHRAE, 1976, *Thermophysical Properties of Refrigerants*, Atlanta, USA, pp.171-175

Box, G.E.P., Hunter, W.G., Hunter, J.S., 1978, *Statistics for Experimenters – An Introduction to Design, Data Analysis and Model Building*, John Wiley & Sons, New York, USA

Churchill, S.W., 1977, Friction-Factor Equation Spans All Fluid-Flow Regimes, *Chem. Eng.*, No.7, pp.91-92

Hermes, C.J.L., Marques, M.E., 2002, *Patent PI 0203675-4*

Karatas, H., Dirik, E., Derbentli, T., 1998, An Experimental Study of Air-Side Heat Transfer and Friction Factor Correlations on Domestic Refrigerator Finned-Tube Evaporators Coil, *7th Int. Ref. Conf. at Purdue*, pp.465-470

Lee, T.-H., Lee, J.-S., Oh, S.-Y., Lee, M.-Y., Lee, K.-S., 2002, Comparison of Air-Side Heat Transfer Coefficients of Several Types of Evaporators of Household Freezer/Refrigerators, *9th Int. Ref. Conf. at Purdue*, R16-5

McAdams, W.H., 1958, *Heat Transmission*, McGraw-Hill, New York, USA

McLinden, M.O., Klein, S.A., Lemmon, E.W., Peskin, A.P., 1998, *REFPROP Software Version 6.0*, NIST Standard Reference Database 23, Gaithersburg, MD, USA

McQuinston, F.C., Parker, J.D., 1994, *HVAC Analysis and Design*, John Wiley & Sons, New York, USA

Melo, C., Piucco, R.O., Waltrich, M., 2004, *Performance Evaluation of No-Frost Evaporators*, Research Report for Multibras Appliances S.A., Federal University of Santa Catarina, Florianópolis, SC, Brazil (in Portuguese)

Wongwises, S., Disawas, S., Kaewon, J., Onurai, C., 2000, Two-Phase Evaporative Heat Transfer Coefficients of Refrigerant HFC-134a Under Forced Flow Conditions in a Small Horizontal Tube, *Int. Comm. Heat & Mass Transfer*, Vol.27, No.1, pp.35-48

ACKNOWLEDGEMENTS

The authors would like to thank *Multibrás Appliances S.A.* for sponsoring this research, in particular Messrs. M. E. Marques and F. L. Freitas Filho. The financial support from Brazilian funding agencies *CNPq* and *CAPES* are duly acknowledged. The authors are also grateful to Messrs. P. O. Duarte and R. O. Piucco for their valuable contributions.